Available online at www.sciencedirect.com
SCIENCE DIRECT®
Catalysis Today 93–95 (2004) 183–190
CATALYSIS TODAY
www.elsevier.com/locate/cattod

Selective oxidation of CO over CuO-CeO_2 catalyst: effect of calcination temperature

C.R. Jung [a], J. Han [b], S.W. Nam [b], T.-H. Lim [b], S.-A. Hong [b], H.-I. Lee [a,*]

[a] *School of Chemical Engineering and Research Center for Energy Conversion and Storage, Seoul National University, Seoul 151-744, Republic of Korea*
[b] *Fuel Cell Research Center, Korea Institute of Science and Technology, Seoul 136-791, Republic of Korea*

Available online 3 July 2004

Abstract

CuO-CeO_2 catalysts were prepared by a conventional co-precipitation method and tested for the selective oxidation of carbon monoxide in the presence of excess hydrogen and carbon dioxide. N_2 adsorption results showed that the BET surface area and pore volume of the CuO-CeO_2 catalyst decreased with increase of calcination temperature whereas average pore diameter increased. From the results of XRD and XPS, we determined the oxidation state of copper in the catalyst. With the increase of calcination temperature, cupric oxide was formed near the surface of the catalyst at first and then appeared on the surface of the catalyst, indicating that the CuO-CeO_2 catalyst was in the form of a solid solution and cupric oxide was formed due to phase separation which then migrated to the surface of the catalyst with the increase of calcination temperature. CO chemisorption data exhibited the amounts of CO uptake of the CuO-CeO_2 catalyst. The amount of reversible CO uptake showed a volcano curve with calcination temperature. The CuO-CeO_2 catalyst batch which was calcined at 700 °C had the best activity because this catalyst formed the most stable state of Cu–Ce–O solid solution and could chemisorb CO reversibly.

Keywords: Selective oxidation of carbon monoxide; Cu–Ce–O solid solution; Copper; Ceria; Calcination temperature

1. Introduction

Fuel cells are considered to be the propulsion system of the near future, since they can produce electricity with substantially less impact on the environment, and possess the necessary specific power, power density and durability to replace conventional internal combustion engines from many of their current applications [1].

Among the various types of fuel cells, H_2-fueled polymer electrolyte membrane fuel cell (H_2-PEMFC) seems to be the most technically advanced energy conversion system for such a purpose [2]. H_2-PEMFC has several advantages such as: (i) low operating temperature, (ii) high power density, and (iii) rapid start up.

While hydrogen is the best fuel for PEMFC, there are serious problems associated with the distribution and storage of hydrogen. A promising way to overcome these problems is to produce the hydrogen feed gas on-board the vehicle, in a fuel-processing unit, by converting a conventional fuel such as natural gas, gasoline or methanol to a hydrogen-rich gas mixture [2]. This can be done either by steam reforming or by autothermal reaction. In either case, the resulting gas mixture contains significant amounts of carbon monoxide and it is further processed in a water gas shift reactor. In this way the gas stream becomes richer in hydrogen and the concentration of carbon monoxide drop to around 1 vol.%, a typical composition being: 45–75 vol.% H_2, 15–25 vol.% CO_2, 0.5-2 vol.% CO, a few vol.% H_2O and N_2 [3,4]. Unfortunately, even this low CO concentration cannot be tolerated by the PEMFC, which is highly sensitive towards trace CO contamination in the H_2 feed gas. It is thus imperative to purify further the hydrogen feed gas, reducing the CO concentration to below 10 ppm [2,5,6].

Among the various options available, the selective oxidation of CO with oxygen or air is undoubtedly the most straightforward, simplest and cost effective one [2,7]. In the last few years, many researchers have developed catalysts which could selectively oxidize CO in the presence of excess hydrogen and carbon dioxide.

The catalysts proposed for selective oxidation process are noble metal-based, such as alumina-supported platinum-group metal catalysts [7,8], zeolite-supported platinum

* Corresponding author. Tel.: +82 2 880 7072; fax: +82 2 888 7295.
E-mail address: hilee@snu.ac.kr (H.-I. Lee).

0920-5861/$ – see front matter © 2004 Elsevier B.V. All rights reserved.
doi:10.1016/j.cattod.2004.06.039

catalysts [9], and metal oxide-supported gold catalysts [10–13]. Recently, CuO-CeO_2 oxide catalyst was proposed as a candidate for the selective oxidation of CO in the presence of excess hydrogen [3,14] because this catalyst is more active and selective than Pt-group-based catalysts at lower reaction temperatures.

Recently, Avgourpoulos et al. [3] reported that CuO-CeO_2 catalyst had the same activity as that of Pt/Al_2O_3 catalyst because of strong interaction between CuO and CeO_2. Other researchers reported [15,16] that in the CuO-CeO_2 system, because the catalyst had a strong interaction due to the presence of highly dispersed CuO on the surface of CeO_2 support and the formation of Cu–Ce–O solid solution, the CuO-CeO_2 catalyst showed a high activity for CO oxidation.

In the present study, we prepared a CuO-CeO_2 catalyst by a co-precipitation method using NH_4OH as a precipitant. We prepared the CuO-CeO_2 catalyst with different calcination temperatures, and investigated the catalytic properties for the selective oxidation of CO in the presence of excess hydrogen and carbon dioxide. Through the characterization of CuO-CeO_2 catalyst, we investigated the active site and tried to identify any factor which aids the catalytic activity.

2. Experimental

2.1. Preparation of catalyst

The CuO-CeO_2 catalyst was prepared by co-precipitation. Aqueous solutions of $Cu(NO_3)_2{\cdot}3H_2O$ (Shinyo), $Ce(NO_3)_3{\cdot}6H_2O$ (Kanto) and NH_4OH (Acros) were gradually and simultaneously added into a continuously stirred flask with distilled water. The reaction mixture was kept at 80 °C. After a period of 1 h, the resulting precipitate was filtered, washed with hot water, and then dried under static air at 75 °C for 12 h. The Cu content of the sample, as determined by atomic absorption spectroscopy (AAS), was 5.1 wt.%.

2.2. Apparatus and method used for activity measurement

The catalytic tests were carried out in a conventional flow, fixed-bed reactor at atmospheric pressure. A quantity of 250 mg of catalyst and a total flow rate of the reaction mixture equal to 156 $cm^3\,min^{-1}$ ($W/F = 0.09\,g\,s\,cm^{-3}$) was used for each run. The reaction mixture consisted of 0.8% CO, 23.5% CO_2, 3.8% air and the balance of H_2.

The effect of H_2O was investigated by the addition of 10 vol.% H_2O in the feed. An excess of oxygen was used for the selective oxidation experiments ($[O_2]/[CO] = 2$).

A CO analyzer made by SIEMENS was used for the analysis of CO, CO_2 and O_2. Methane and hydrogen contents were analyzed by gas chromatography, but methane was not detected under our experimental conditions.

The CO conversion was calculated based on the CO consumption as follows:

$$\text{Conversion} = \frac{[CO]_{in} - [CO]_{out}}{[CO]_{in}} \times 100\,(\%)$$

The calculation of CO conversion was based on the CO consumption, because of the large error in the quantification of small changes in the CO_2 concentration.

The selectivity was calculated from the oxygen mass balance as follows:

$$\text{Selectivity} = \frac{0.5([CO]_{in} - [CO]_{out})}{[O_2]_{in} - [O_2]_{out}} \times 100\,(\%)$$

2.3. Catalyst characterization

2.3.1. Thermogravimetric and differential thermal analysis (TG-DTA)

TG-DTA analysis of the catalyst precursor was carried out using a MAC Science TG-DTA 2000 thermal analyzer in the range of 30–1000 °C in air atmosphere. The heating rate was maintained at 5 °C/min.

2.3.2. Specific surface area and pore size distribution

BET surface area, pore volume and pore size distribution were measured by nitrogen adsorption-desorption at 77 K using a Micromeritics ASAP 2010 instrument. Pore volume and pore size were determined by applying the Barrett–Joyner–Halenda method [17] to the desorption branch of the isotherm. Prior to the measurements, those samples were evacuated at 200 °C for at least 2 h.

2.3.3. X-ray powder diffraction (XRD)

X-ray diffraction measurement was made using a Rigaku D/MAX-IIIA X-ray diffractometer with a scan speed of 10^o/min, in the scan range of 20–80° using Cu Kα as an X-ray source.

The mean crystallite sizes (D_β) of the CeO_2 grains were determined from line-broadening measurements on the ⟨1 1 1⟩ peak of CeO_2, using the Scherrer equation,

$$D_\beta = \frac{K\lambda}{\beta \cos\theta}$$

where λ is the synchrotron wavelength, K is the particle shape factor, taken as 0.94 for spherical particles, β is the full-width at half maximum height (FWHM) in radians. The β–values were carefully determined by a least-square fit of a Gaussian function.

2.3.4. Temperature-programmed reduction (TPR)

The TPR was carried out by using 10% hydrogen in nitrogen as a reducing gas in a conventional TPR reactor. The reactor was made up of a 4 mm i.d. quartz tube with catalyst sample of 70 mg mounted on loosely packed quartz wool. Before entering the reactor, the reactant gas was purified by passing through an oxygen and moisture trap. The outlet of the reactor was connected to a glass column packed with molecular sieve of 5 in. in order to remove the moisture produced from the reduction reaction. The flow rate of

the reducing gas was kept at 25 ml/min using a mass flow controller. The temperature of the reactor was raised from room temperature to 600 °C at the rate of 10 °C/min by a temperature programmable controller. The rate of hydrogen consumption was measured by a thermal conductivity detector and recorded by an on-line personal computer.

2.3.5. X-ray photoelectron spectroscopy (XPS)

The XPS analysis of the catalyst was carried out at room temperature with a VGESCALAB 220i-XL spectrometer (Fisons). The residual pressure in the spectrometer was in the range 1.3–6.5 × 10^{-7} Pa. A monochromated Al anode (energy of the Al Kα line 1486.6 eV), powered at 10 keV and 20 mA, was used for X-ray production. The binding energies were calculated with respect to the C 1s peak at 284.5 eV. Deconvolution of the peaks was done with the best fitting routine of the XPSPEAK program.

2.3.6. CO chemisorption

In a Micromeritics ASAP 2010C apparatus, CO chemisorption analysis was performed under static volumetric conditions and the samples were heat-treated in situ in He at 350 °C prior to the measurements. The sample was evacuated at 360 °C for 1.5 h and left to cool to 35 °C. The chemisorption isotherm was obtained by measuring the adsorbed amount of CO for pressures varying from 100 to 500 mmHg. Assuming a stoichiometry of one CO molecule per surface metal atom, the dispersion was calculated. After completing the initial analysis, the reversibly adsorbed gas was evacuated and the analysis was repeated to determine the chemisorbed molecules only.

3. Results and discussion

In our previous studies, we found that the selective CO oxidation activity was the highest for a CuO loading of 5.1 wt.% and decreased for higher CuO loading, and therefore the CuO loading was maintained at this level.

In order to determine the calcination temperature, TG-DTA analysis of CuO-CeO_2 catalyst precursor was carried out. TG curve of the catalyst precursor is given in Fig. 1. One sharp weight loss was observed in the TG curve of the catalyst precursor and the weight loss was continuous up to 520 °C and was about 5% with regard to the total weight of the catalyst precursor. However, we could not observe any peak in the DTA curve, indicating that there was no exothermic or endothermic reaction occurring. Thus, it was not difficult to infer from the results of TG-DTA analysis that the weight loss was caused by the evaporation of residual water or solvent. From these results, it was clear that the calcination temperature should be above 500 °C, and thus, we selected the calcination temperatures to be 500, 600, 700, 800 and 900 °C, respectively.

Using the catalysts prepared at different calcination temperatures, reaction experiment for the selective oxidation of

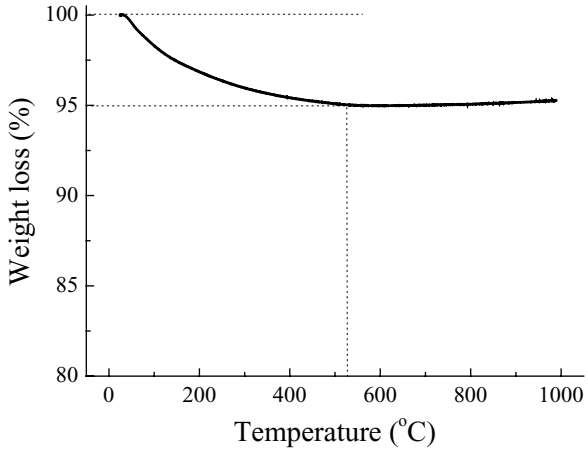

Fig. 1. TG curve of 5.1 wt.% CuO-CeO_2 catalyst precursor.

CO was carried out in the presence of excess hydrogen and carbon dioxide. Fig. 2 presents the conversion of CO (A) and selectivity for CO_2 (B) over CuO, CeO_2 and CuO-CeO_2 catalysts. The activity of selective oxidation over either CuO or CeO_2 was quite low in the low temperature region (below 200 °C), but the activity of the prepared CuO-CeO_2 catalyst was much higher than that of CuO or CeO_2. This increase of catalytic activity might be caused due to the strong interaction between CuO and CeO_2 as published previously [18]. The catalytic activity of the CuO-CeO_2 catalyst showed a volcano curve with calcination temperature and the catalyst which was calcined at 700 °C had the best activity while the selectivity over CuO-CeO_2 catalyst increased with calcination temperature.

The catalytic activity of the prepared catalysts were also examined in different gas composition; without CO_2 (replaced by N_2) and with H_2O (10% steam). When N_2 was supplied, the temperature which showed the maximum catalytic activity (T_{max}) was shifted to a lower temperature by about 20–30 °C. And as the steam was added, T_{max} was shifted to a higher temperature by about 10–20 °C. Because of hindrance of reactant adsorption and product desorption, the catalytic activity decreased in the presence of CO_2 or H_2O, in the feed. Consequently, the CuO-CeO_2 catalysts showed different activities for the selective oxidation reaction with the different calcination temperatures.

In order to find the correlation between the calcination temperature and the catalytic activity, several different characterization methods were employed. First, the physical properties of CuO-CeO_2 catalyst such as specific surface area, pore volume and average pore diameter were measured and the results are summarized in Table 1. Fig. 3 shows the adsorption–desorption isotherms and the pore size distribution patterns of CuO-CeO_2 catalyst prepared at different calcination temperatures. With the increase of calcination temperature, the area with the gourd shape decreased, indicating that the micro-pores in the range of 1–4 nm collapsed sharply, thereby leading to a decrease in pore volume and BET surface area whereas the average

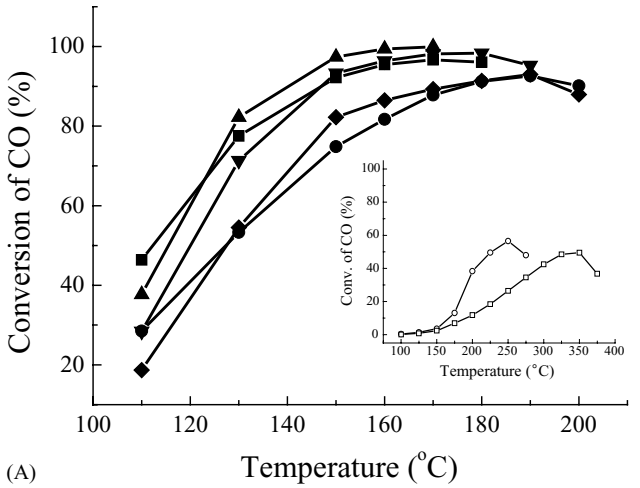

(A)

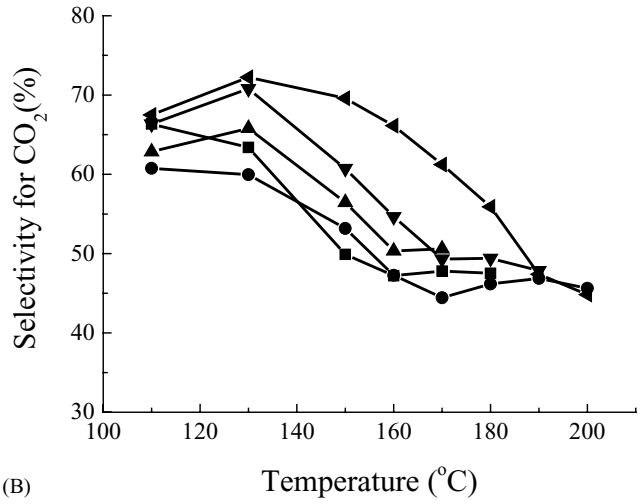

(B)

Fig. 2. (A) conversion of CO and (B) selectivity for CO_2 over 5.1 wt.% CuO-CeO_2 catalyst prepared at different calcination temperature: 500 (●), 600 (■), 700 (▲), 800 (▼), and 900 °C (◆). The inset shows the conversion of CO over pure CuO (○) and CeO_2 (□).

pore diameter increased. However, we could not find any correlation between the physical properties of CuO-CeO_2 catalyst and the catalytic activity.

Fig. 4 shows the XRD patterns of CuO-CeO_2 catalyst with different calcination temperatures. The XRD patterns showed that a fluorite-type oxide structure of CeO_2 was

Table 1
Physical properties of CuO-CeO_2 catalyst prepared at different calcination temperatures

Calcination temperatures (°C)	S_{BET} (m^2/g)	V (cm^3/g)	D (nm)	d (nm)
500	78	0.08	4.0	11.0
600	50	0.06	4.7	12.1
700	22	0.05	8.1	24.3
800	12	0.03	10.4	45.5

S_{BTE}: BET surface area, V: pore volume, D: average pore diameter d: crystallite size calculated by Scherrer equation from XRD data.

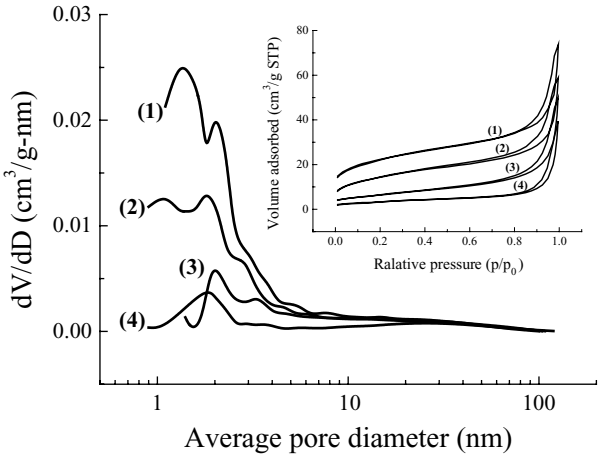

Fig. 3. Adsorption-desorption isotherm and pore size distribution of 5.1 wt.% CuO-CeO_2 catalyst prepared at different calcination temperature: (1) 500, (2) 600, (3) 700, and (4) 800 °C.

present in all samples. When the calcination temperature was below 700 °C, XRD characteristic peaks of CuO and Cu_2O, which appear in the region of 35–40°, were not detected in any of the samples (Fig. 4(B)). Copper oxide peaks were not observed in the XRD patterns of the CuO-CeO_2 catalyst probably due to the formation of Cu–Ce–O solid solution [19] or highly dispersed CuO on the surface of ceria support.

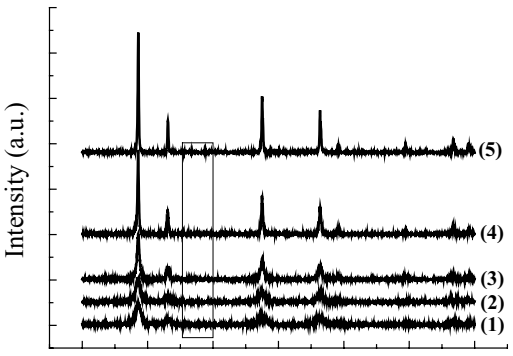

(A)

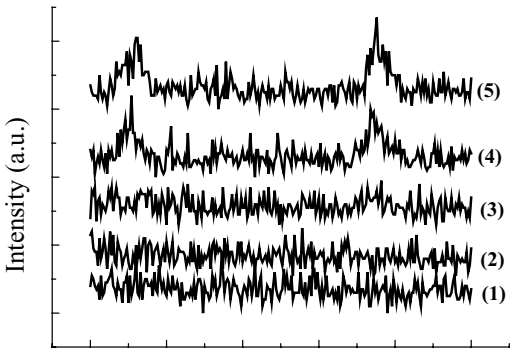

(B)

Fig. 4. XRD patterns of (A) wide range and (B) narrow range for 5.1 wt.% CuO-CeO_2 catalyst with different calcination temperatures: (1) 500, (2) 600, (3) 700, (4) 800, and (5) 900 °C.

In case of highly dispersed CuO, the active site for the selective oxidation of CO should be the highly dispersed CuO on the surface of ceria support, but this does not explain the trend of the catalytic activity. As mentioned later in the TPR profiles of the CuO-CeO_2 catalyst, with the increase of calcination temperature, the amount of highly dispersed CuO was decreased unlike the catalytic activity which showed a volcano curve.

In case of the Cu–Ce–O solid solution, we should detect the change of ceria peak with the increase of calcination temperature. However, no observable shift in the diffraction peaks of CeO_2 could be found in any XRD patterns of the CuO-CeO_2 catalyst. Sedmak et al. [20] reported that cuprous oxide Cu_2O, which has a primitive cubic lattice and an ionic radius of Cu^{+1} equal to 0.115 nm, and CeO_2, which has a fluorite structure with an ionic radius of the Ce^{+4} ion equal to 0.111 nm can form a substitution solid solution. In this case, the formation of the solid solution causes little change in the lattice parameter so that no observable XRD peak shift can be detected. However, from the XRD result of CuO-CeO_2 catalyst, we could not confirm the chemical state of copper oxide in the CuO-CeO_2 catalyst. Thus, XPS was carried out to confirm the chemical state of copper oxide, and more discussion on the chemical state will be presented in the later part of this section.

On the other hand, as the calcination temperature was above 800 °C, we could observe the XRD peak of CuO. This indicated that in the case of highly dispersed CuO, CuO was formed by sintering due to high temperature calcination, and that in the case of Cu–Ce–O solid solution, CuO appeared to be formed by phase separation from the Cu–Ce–O solid solution, as indicated by the appearance of XRD peaks of CuO.

CeO_2 crystallite size was calculated using the XRD data by Scherrer equation, and the results are presented in Table 1. Crystallite size of CeO_2 (1 1 1) remained nearly constant until the CuO-CeO_2 catalyst was calcined at 600 °C, and above 700 °C, it increased with the increase of calcination temperature. As the calcination temperature was raised above 700 °C, CeO_2 first underwent sintering and thereafter, the surface area and pore volume of the catalysts decreased.

Fig. 5 shows the XRD patterns of CuO-CeO_2 catalyst with varying amount of CuO loading and calcination temperature. When the CuO-CeO_2 catalyst was calcined at 700 °C, CuO peak was observed only at a CuO loading of 8.6 wt.%, but not in the sample with 5.1 wt.%. However, when the CuO-CeO_2 catalyst was calcined at 800 and 900 °C, though the amounts of CuO loading is little, that is, 2.8 wt.%, XRD peaks due to the CuO were detected. In the case of CuO-CeO_2 catalyst which was prepared by co-precipitation by Liu and Flytzani-Stephonopoulos [15], the amount of CuO loading is more than 15 at.% and the XRD peaks corresponding to CuO were observed. In our work, as the CuO loading is 8.6 wt.%, the amount of Cu ion is 16.9 at.% and hence the XRD peaks due to the CuO were detected in all samples calcined at 700 °C and above.

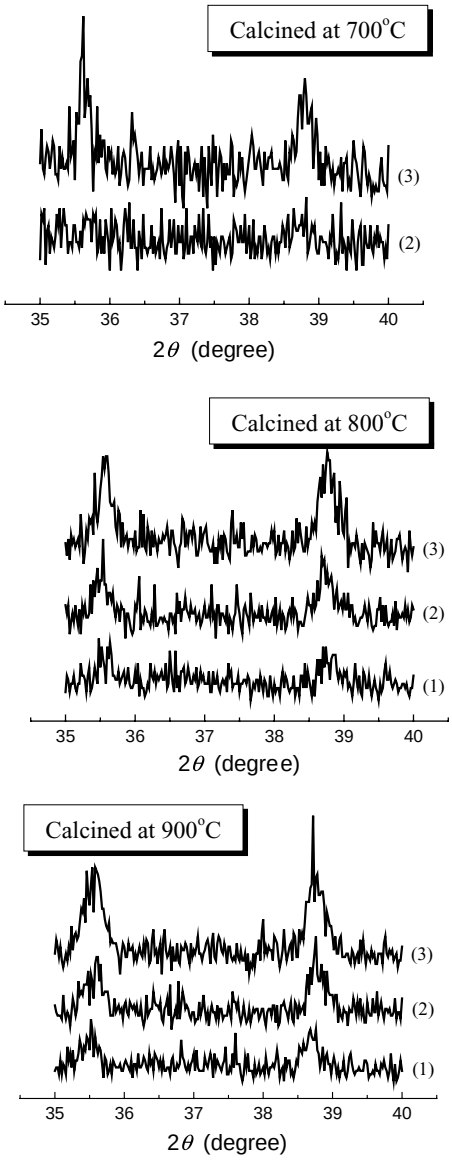

Fig. 5. XRD patterns of 5.1 wt.% CuO-CeO_2 catalyst with the different amount of CuO loading at three different calcination temperatures: (1) 2.8, (2) 5.1, and (3) 8.6 wt.%.

To confirm the oxidation state of copper and cerium in the CuO-CeO_2 catalyst, we carried out X-ray photoelectron spectroscopy (XPS), and Table 2 compares the Cu $2p_{3/2}$, Ce $3d_{5/2}$ and O 1s XPS binding energy of the CuO-CeO_2

Table 2
XPS binding energies of Cu, Ce and O in the CuO-CeO_2 catalyst prepared at different calcination temperatures

Calcination temperatures (°C)	Binding energy (eV)		
	Cu $2p_{3/2}$	Ce $3d_{5/2}$	O 1s
600	932.0	881.7	528.7
700	931.9	881.7	528.9
800	932.1	881.7	528.6
900	933.2	881.7	529.2

Table 3
The oxidation state of copper in the CuO-CeO_2 catalyst prepared at different calcination temperatures

Calcination temperatures (°C)	Near surface[a]		Surface[b]	
	Before reaction	After reaction	Before reaction	After reaction
700	n.d.	n.d.	Cu_2O	Cu/Cu_2O[c]
800	CuO	n.d.	Cu_2O	Cu/Cu_2O[c]
900	CuO	Metallic Cu	CuO	CuO

n.d.: not detected.
[a] The region which was analyzed by XRD.
[b] The region which was analyzed by XPS.
[c] We could not distinguish.

catalyst with different calcination temperatures. The binding energies were calculated with reference to the energy of C 1s peak of contaminant carbon at 284.5 eV. And the binding energy of Cu in the catalyst was calibrated with the XPS analysis of pure CuO and Cu_2O which were purchased from WAKO Pure Chemical Industries, Ltd. as reference materials in order to eliminate the effect of possible photo-reduction. In the XPS results of CuO and Cu_2O, the Cu $2p_{3/2}$ binding energy in the CuO was 933.6 eV and the Cu $2p_{3/2}$ binding energy in the Cu_2O was 932.0 eV.

As the calcination temperature was below 800 °C, Cu $2p_{3/2}$ binding energy of the CuO-CeO_2 catalyst was lower than that of Cu $2p_{3/2}$ in the CuO, and it coincided with Cu $2p_{3/2}$ in the Cu_2O. However, as the CuO-CeO_2 catalyst was calcined at 900 °C, Cu $2p_{3/2}$ binding energy indicated the presence of CuO, that is, the oxidation state of copper in the CuO-CeO_2 catalyst was +2. Ce $3d_{5/2}$ binding energy of CuO-CeO_2 catalyst was 881.7 eV, indicating that the oxidation state of cerium in the catalyst was +4, that is, CeO_2.

From the results of XRD and XPS data, we could summarize the oxidation state of copper in the CuO-CeO_2 catalyst as shown in Table 3. It appears that the oxidation state of copper in the CuO-CeO_2 catalyst changes from cuprous oxide to cupric oxide with the increase of calcination temperature, and the cupric oxide is formed near the surface of CuO-CeO_2 catalyst at first, and then appears on the surface of the CuO-CeO_2 catalyst. This indicates that the CuO-CeO_2 catalyst is formed as a solid solution and with the increase of calcination temperature, CuO is formed near the surface of CuO-CeO_2 catalyst due to phase separation and migrates to the surface of the CuO-CeO_2 catalyst. In the case of highly dispersed CuO on the ceria surface [21], CuO is formed on the surface of the CuO-CeO_2 catalyst because copper on the surface of the CuO-CeO_2 catalyst is easy to mobilize and then appears near the surface of the CuO-CeO_2 catalyst.

Fig. 6 shows the XRD patterns of CuO-CeO_2 catalyst before and after reaction. As the CuO-CeO_2 catalyst was calcined at 700 °C, the XRD peaks for the copper oxide were not observed (not shown in Fig. 6). However, before reaction, the XRD peaks for the CuO were observed with the increase of calcination temperature, and after reaction, the XRD peak for metallic copper was detected as the CuO-CeO_2 catalyst was calcined at 900 °C. In the case of CuO-CeO_2 catalyst which was calcined at 900 °C, though the catalyst remained in air flow during the shut down period, the metallic copper which was formed under the reaction condition was not changed to CuO.

The H_2-TPR profiles of CuO-CeO_2 catalyst with different calcination temperature are shown in Fig. 7. The TPR profiles of the CuO-CeO_2 catalyst which was calcined below 700 °C, showed two reduction peaks in the range at 140–210 °C. But, in the case of CuO-CeO_2 catalyst which was calcined above 800 °C, the profiles of CuO-CeO_2 catalyst showed a single broad peak in the range of

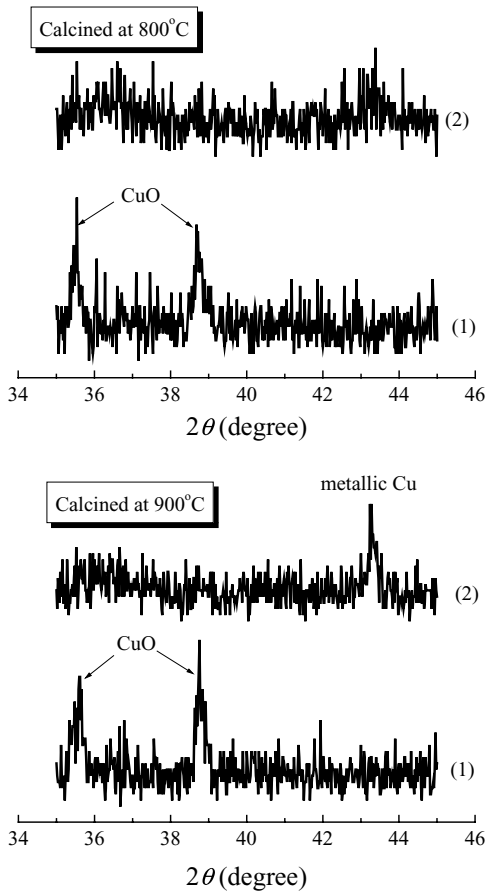

Fig. 6. XRD patterns of 5.1 wt.% CuO-CeO_2 catalyst with the two different calcination temperatures: (1) before reaction and (2) after reaction.

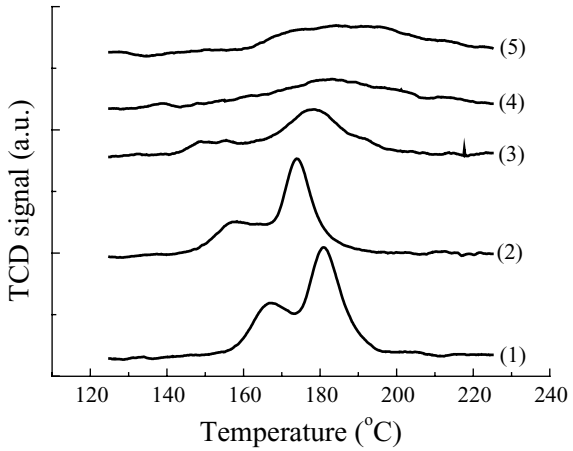

Fig. 7. TPR profiles of 5.1 wt.% CuO-CeO_2 catalyst with different calcination temperatures: (1) 500, (2) 600, (3) 700, (4) 800, and (5) 900 °C.

140–220 °C. With the increase of calcination temperature, the low-temperature peak was shifted to even lower temperature and finally disappeared, and the high-temperature peak area decreases gradually. When calcined above 800 °C, reduction peak of CuO formed by phase separation was overlapped and appeared as a single broad peak in the range 140–220 °C.

Xiaoyuan et al. [18] reported that pure CuO showed a single H_2 reduction peak at 392 °C, whereas in the pure CeO_2, the TPR profile showed two reduction peaks at 430 and 570 °C. They presumed that the low-temperature peak was due to the reduction of CeO_2 surface oxygen, and the high-temperature peak was due to the reduction of bulk oxygen. Two reduction peaks were observed in the CuO/CeO_2 catalyst, and they concluded that the low temperature reduction peak corresponds to small CuO particles which were highly dispersed on the CeO_2 surface and had strong interaction with CeO_2, while the other peak corresponds to larger particles or bulk CuO, which also interacted with CeO_2.

On the other hand, it was reported that reducibility of ceria was enhanced by copper in the Cu-CeO_2 system [15,16,22,23] or by gold in the Au-CeO_2 system [24]. This means that the two reduction peaks appeared due to the reduction of oxygen species in the Cu- or Au-CeO_2 system. In the present work, referring to the catalytic activity, it appears that the two reduction peaks are not due to the reduction of CuO but due to the reduction of oxygen species in the catalyst. Thus, the low-temperature peak is due to the reduction of surface oxygen and the high-temperature peak is due to the reduction of bulk oxygen in the CuO-CeO_2 system. The amounts of reducible oxygen species in the catalyst decreased with calcination temperature, and this result shows a similar trend with the physical properties, such as BET surface area and pore volume of CuO-CeO_2 catalyst.

In order to investigate the correlation between catalytic activity and amount of chemisorbed CO uptake, CO chemisorption analysis was performed and the results were summarized in Table 4. With the increase of calcination temperature, the total amount of CO uptake decreased, and the trend was similar with physical properties such as BET surface area and pore volume, and the amount of reversible oxygen species. However, the amount of reversible CO uptake showed a volcano curve suggesting that the reversible CO uptake on the CuO-CeO_2 catalyst is one of the main factors which affect the catalytic activity.

Table 4
CO uptakes of CuO-CeO_2 catalyst prepared at different calcination temperatures

Calcination temperatures (°C)	CO uptake (cm^3/g)		
	Reversible	Irreversible	Total
500	1.4	10.0	11.4
600	2.6	4.8	7.4
700	2.6	2.8	5.4
800	1.2	0.6	1.8
900	0.6	0.2	0.8

4. Conclusion

In this study, CuO-CeO_2 catalysts were prepared by co-precipitation and tested for selective oxidation of CO in a typical refomate gas composition. The catalytic activities and properties for selective oxidation were found to be strongly influenced by the calcination temperature. All samples of CuO-CeO_2 catalyst formed a Cu–Ce–O solid solution, and with the increase of calcination temperature, CuO was formed due to phase separation, which then migrated to the surface of CuO-CeO_2 catalyst. The catalyst which was calcined at 700 °C for 4 h in air flow, showed the best activity due to the most stable state of Cu–Ce–O solid solution.

Acknowledgements

This work was financially supported by Korea Institute of Science and Technology, and by Korea Science and Engineering Foundation through Research Center for Energy Conversion and Storage.

References

[1] G.P. Gray, J.C. Frost, Energy Fuels 12 (1998) 1121.
[2] R.A. Lemons, J. Power Sources 29 (1990) 251.
[3] G. Avgouropoulos, T. Ioannides, Ch. Papadopoulou, J. Batista, S. Hocevar, H.K. Matralis, Catal. Today 75 (2002) 157.
[4] G. Avgouropoulos, T. Ioannides, Appl. Catal. A: Gen. 244 (2003) 155.
[5] H. Igarashi, T. Fujino, M. Watanabe, J. Electroanal. Chem. 391 (1995) 119.
[6] H.F. Oetjen, V.M. Schmidt, U. Stimming, F. Trila, J. Electrochem. Soc. 143 (1996) 3838.

[7] S.H. Oh, R.M. Sinkevitch, J. Catal. 142 (1993) 254.
[8] M.J. Kahlich, H.A. Gasteiger, R.J. Behm, J. Catal. 171 (1997) 93–105.
[9] H. Igarashi, H. Ushida, M. Suzuki, Y. Sasaki, M. Watanabe, Appl. Catal. A: Gen. 159 (1997) 159.
[10] G.K. Bethke, H.H. Kung, Appl. Catal. A: Gen. 194 (2000) 43.
[11] R.J.H. Grisel, B.E. Nieuwenhuys, J. Catal. 199 (2001) 48–59.
[12] M.J. Kahlich, A. Gasteiger, R.J. Behm, J. Catal. 182 (1999) 430.
[13] W.-S. Shin, C.-R. Jung, J. Han, S.-W. Nam, T.-H. Lim, S.-A. Hong, H.-I. Lee, J. Ind. Eng. Chem. 10 (2004) 302.
[14] G. Avgouropoulos, T. Ioannides, H. Matralis, J. Batista, S. Hocevar, Catal. Lett. 73 (2001) 33.
[15] W. Liu, M. Flytzani-Stephonopoulos, J. Catal. 153 (1995) 304.
[16] W. Liu, M. Flytzani-Stephonopoulos, Chem. Eng. J. 64 (1996) 283.
[17] E.P. Barrett, L.G. Joyner, P.P. Halenda, J. Am. Chem. Soc. 73 (1951) 373.
[18] J. Xiaoyuan, L. Guanglie, Z. Renxian, M. Jianxin, C. Yu, Z. Xiaoming, Appl. Surface Sci. 173 (2001) 208.
[19] C. Lamonier, A. Ponchel, A. D'Huysser, L. Jalowiecki-Duhamel, Catal. Today 50 (1999) 247.
[20] G. Sedmak, S. Hoèevar, J. Levec, J. Catal. 213 (2003) 135.
[21] G.-H. Lee, M.S. Lee, G.-D. Lee, Y.-H. Kim, S.-S. Hong, J. Ind. Eng. Chem. 8 (2002) 572.
[22] Y. Li, Q. Fu, M. Flytzani-Stephonopoulos, Appl. Catal. B: Environ. 27 (2000) 179.
[23] Lj. Kundakovic, M. Flytzani-Stephonopoulos, Appl. Catal. A: Gen. 171 (1998) 13.
[24] Q. Fu, S. Kudriavtseva, H. Saltsburg, M. Flytzani-Stephonopoulos, Chem. Eng. J. 93 (2003) 41.